

# Velocity Profile Variabilities at a Tidal-Stream Energy Site Facing Open Sea (Raz Blanchard, France)



Lucille Furgerot, Pascal Bailly du Bois, Mehdi Morillon, Yann Méar  
and Emmanuel Poizot

**Abstract** The Alderney Race is one of the most powerful current in Europe (up to 5 m/s during spring tide). Considering these important currents, this site has been identified to extract energy from the tide with installation of tidal turbines. However, this area is facing open sea to the west and thus strong wind can generate significant wave height interplaying with the tidal currents, which is a critical point for the dimensioning of the tidal turbines. This chapter deals with in situ measurements of waves and currents in Alderney Race.

**Keywords** Wave-current interactions · Alderney race · ADCP measurements · Velocity vertical profiles

## 1 Introduction

The Alderney Race (French Raz Blanchard) current occurring between Normandy (France) and the Channel Sea Islands (UK) is one of the most powerful current in Europe (5 m.s<sup>-1</sup> during spring tide). This current, give opportunity to extract energy from the tide with installation of tidal turbines (Bahaj and Myers, 2004). However, as the Alderney Race area is facing open sea to the west, strong wind can generate significant wave height ( $H_s$ ) interplaying with the tidal currents. The HYD2M project aims to improve the tidal energy estimation by combining an original dataset of in-situ measurements with the development of 3D numerical model including wind and waves effects. We have carried out 5 campaigns in the Alderney Race with water level, current, waves and wind measurements (from April 2017 to July 2018). The high temporal resolution of our dataset (up to 2 Hz, for most of the campaigns

---

L. Furgerot (✉)

LUSAC Laboratory, University of Caen Normandy, Cherbourg en Cotentin, France  
e-mail: [lucille.furgerot@hotmail.fr](mailto:lucille.furgerot@hotmail.fr)

P. Bailly du Bois · M. Morillon  
IRSN-LRC, Cherbourg en Cotentin, France

Y. Méar · E. Poizot  
CNAM Intechmer, Cherbourg en Cotentin, France

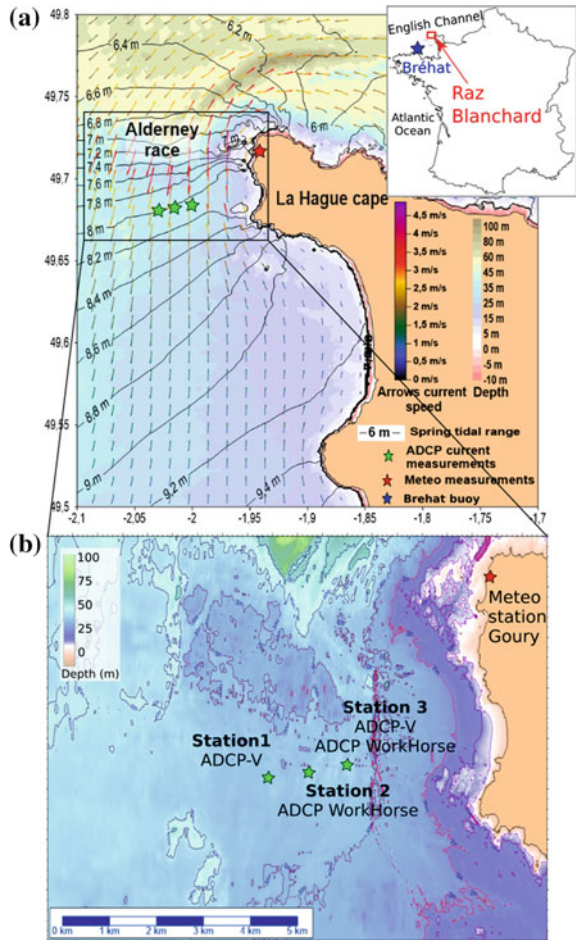
© Springer Nature Singapore Pte Ltd. 2020  
K. D. Nguyen et al. (eds.), *Estuaries and Coastal Zones in Times  
of Global Change*, Springer Water,  
[https://doi.org/10.1007/978-981-15-2081-5\\_10](https://doi.org/10.1007/978-981-15-2081-5_10)

and devices) allows the study of the interactions between waves and tidal currents. Since measurements are still in progress, this chapter focuses on preliminary results, including (i) a description of meteorological and dominant waves conditions, (ii) a description of the tidal currents dynamic, (iii) a study of averaged vertical profiles variability, and (iv) a preliminary discussion concerning the influence of the waves on the vertical profiles, mainly dominated by tidal currents.

## 2 Study Site: Alderney Race

The Alderney Race tidal current is located in the northern part of the Normandy-Brittany Gulf (France) between the Alderney Island and the La Hague Cape (Fig. 1).

**Fig. 1** a Location map with simulated tidal amplitude (spring tide), direction of maximum currents, as well as current-measurement locations; b Zoom on the measurement area showing the location of 3 ADCP stations and the meteorological station



Currents are related to the tidal wave coming from the Atlantic Ocean. The tidal wave amplitude increases when it crosses the continental shelf (500 km westward) and subsequently when this wave is reflected by the Cotentin Peninsula, acting as a barrier. This creates a significant tidal range (more than 14 m near the Mont Saint Michel bay) in the Normandy-Brittany Gulf causing strong tidal currents. From North to South of the La Hague Cape, the maximum tidal range varies from 6 m to 11 m (5 km apart). This leads to a significant slope of the water (black contours—Fig. 1) that generates the strong currents. In addition, the shallow depth (<50 m, colors Fig. 1) and the presence of the Alderney island creates a funnel effect, increasing the flow (arrows on Fig. 1). Previous studies mainly focus on numerical models (Bailly du Bois and Dumas 2005; Neill et al. 2011; Coles et al. 2017), validated by local and punctual measurements using in situ current meters. They have identified an area with maximum currents velocities (Bailly du Bois et al. 2012), located between the La Hague Cape and the Alderney Island (red arrows Fig. 1). In this area, the current magnitude ( $U_{mag}$ ) can reach  $5 \text{ m}\cdot\text{s}^{-1}$  during the high spring tides. The tide is commonly described as an asymmetric tide, dominated by a NNE-directed flow current, estimated to be 3% stronger than the SSW-directed ebb current (Thiébot et al. 2015). The current inversion during the transition between the ebb and the flood is relatively fast, around 15 min. Because of strong in situ technical constraints for instrumentation (strong currents, short time window with relatively low currents during the inversion, etc) only few studies have been carried out over long periods.

### 3 Materials and Methods

Since the 21th April, 2017, we have carried out 5 campaigns on the Thalia and Côtes de la Manche research vessel (CNRS-INSU, France) that allowed the measurement of water level and currents along vertical profiles, at three different stations (Fig. 1). These stations are located along an E-W profile and are named respectively stations 1, 2 and 3 (from West to East). They are located south of the strongest current zone for technical constraints, particularly the difficulty to find plane areas (rocks with one meter mean size in the north). We deployed on the bottom (made of boulders and blocks) one structure for each station, where ADCP (Acoustic Doppler Current Profiler) have been fixed. These structures have been designed specifically to resist to strong currents and to protect the sensors from possible impacts of pebbles or other particles, moving close to the bottom (bottom mainly consists of sand and pebble (Foveau et al. 2017 confirmed by photos). The maximum immersion depth was around 40 m. Technical problems occurred related to the recovery of the structures with an automatized remote buoy. Despite the technical issues, a huge amount of data has been recorded (up to 240 days of data corresponding to ~20 million entries in the database). We have also collected meteorological (Goury semaphore, Météo

**Table 1** ADCP configurations for the three measurements station (stations located in Fig. 1)

	April	June	September	October	February
Station 1	ADCP-V 2Hz (burst of 20 min every hour)				
Station 2	ADCP Workhorse Average data of 1Hz over 5min		ADCP Workhorse Continuous 1Hz measurements		ADCP Workhorse 1Hz (burst of 2min every each 5min)
Station 3	No data		ADCP Workhorse Continuous 1Hz measurements		ADCP-V Continuous 2Hz measurements

France) and wave parameters (French buoy network Candhis) in open access sources in order to complete our database.

### Tidal Currents and Elevation

Pressure sensors from the ADCP allow the measurement of the surface variations above each offshore structure.

Measurements of currents along vertical profiles using ADCP have been carried out simultaneously for the three structures in the three locations (Fig. 1). During a typical campaign at sea, we have recovered the structures, collected the data and re-immersed the structures. During each data recovery, we checked if the ADCPs were still operating. The measurement cells size is 1 m high and the first cell is located from 1.5 to 2 m above the sea floor.

We used two different types of ADCP models from RDI®: (i) an ADCP-V 500 kHz and (ii) an ADCP Workhorse 600 kHz. The model of ADCP deployed in each station and their acquisition frequency varies through time because of one accidental lost and adjustment of the acquisition frequency according to the batteries and memory capacity (Table 1).

Because of the lost and other problems in station 3 during the first period, in this chapter, we present only the data from stations 1 and 2.

Each ADCP measures the current velocity along three axes, directed north-south ( $V$ , positive values northward), east-west ( $U$ , positive values eastward) and vertically ( $W$ , positive values upward) for each point, along vertical profiles. The two main velocity components ( $U$  and  $V$ ) allow the calculation of the velocity vectors ( $U_{mag}$ ). The direction ranges from 0 to 360°, with 0° northward. The data were averaged over a period of 5 min ( $\bar{U}_{mag}$ ) to allow easy viewing and to study the velocity evolution during tidal cycles (Fig. 3). High-frequency raw data (1 Hz and 2 Hz) are presented at the end of this chapter (Fig. 5). After a general analysis, the vertical velocity profiles have been compared for eight cases of  $U_{mag}$  averaged on the water column to study the variability of profiles (Lewis et al. 2017). This analysis of profile shape has been made by using the equation:

$$V(z) = V_0 \left( \frac{z}{d} \right)^{1/\alpha} \quad (1)$$

which allows to analyzed the variability of the  $\alpha$  coefficient.  $V_0$  corresponds to the surface velocity,  $d$  represent the depth of the water column and  $z$  the distance from the bottom for each point. The use of this method could be discussed, as the higher measuring cell of the ADCPs is located at 3 m below the surface. The  $\alpha$  coefficient have been tested for a range of values from 1 to 15, for each intervals of 0,1 and the best coefficient have been estimated from linear regression fit of Log Log representation of velocity. This analysis takes into account the velocity variations in the boundary layer for important depths. According to Thiébaud and Sentchev (2017) and Soulsby (1977), the boundary layer may extend over tens of meters in high hydrodynamic conditions.

### Waves Data

For the wave analyses, we have collected open source data from the buoy located 20 km North of Bréhat (Candhis network). The ADCP-V (initially station 1 and 3 and then only station 1—Fig. 1), allowed the calculation of the main waves parameters, using different methods:  $H_s$  (significant height),  $T_s$  (significant period) and  $D_p$  (main peak direction). We chose the orbital velocities method. According Wiberg and Sherwood (2008), this method is assumed to be reliable, especially when the free surface spectral analyses cannot be done, which is the case in the present chapter, due to pressure sensor problems.

### Wind Intensity and Direction

The wind data used in this study are measured by the Météo-France at semaphore in Goury (Fig. 1). Each data corresponds to an average over a period of 6 min, at an altitude of 10 m. The wind direction has been measured with a resolution of  $10^\circ$ .

## 4 Preliminary Results

### General Meteorological and Waves Climates During Campaigns

One main wave regime has been identified from both Bréhat and our data set (Fig. 2a), with waves coming from the West ( $N280^\circ$  to  $N290^\circ$ ).

A secondary wave regime has been found in the Bréhat data (Fig. 2a), from the north and on our data (Fig. 2a) coming from the northeast but is negligible compared to the main regime. The dominant wind comes from the southwest (from  $N180^\circ$  to  $N270^\circ$ ) and less frequently from the east (Fig. 2a). The waves from the principal regime come from the Atlantic Ocean where the fetch length is very large. In the other directions, the fetch length is not enough important to generate measurable significant swell waves. The directions show a more important dispersion from the southwest to northwest compared with Bréhat. This could be due to wave refraction on the islands or due to shallower depth. During the acquisition campaigns, five neap/spring tide cycles have been recorded. The tidal range fluctuated between 1.8 m and 7.8 m

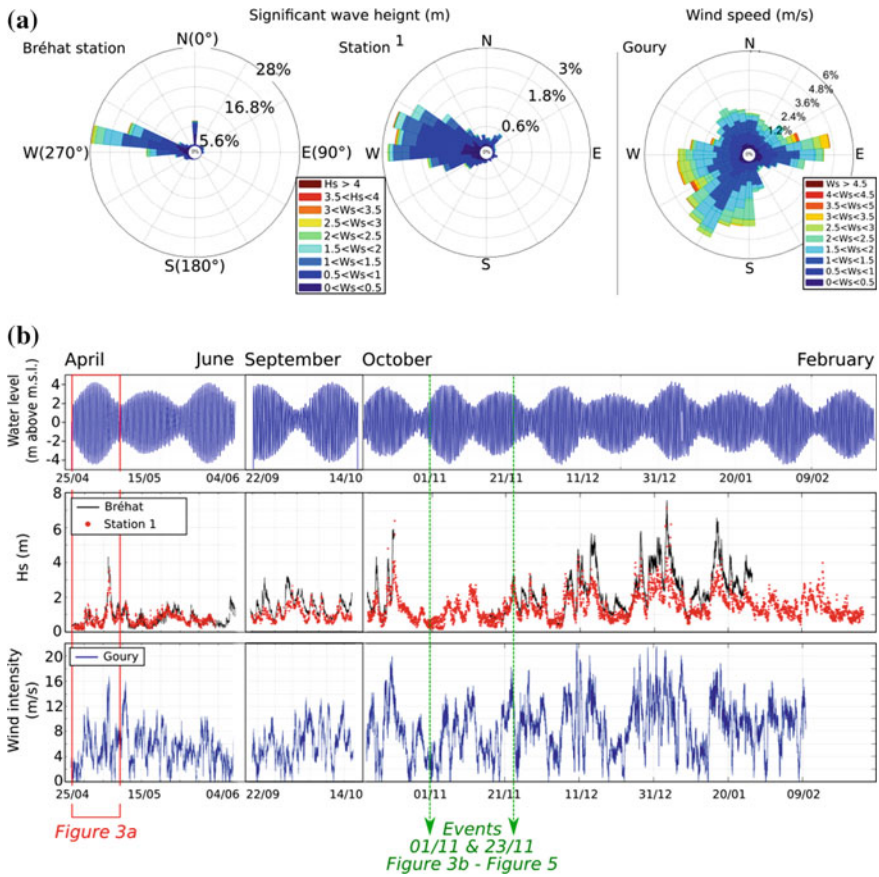


**Fig. 2** Waves and wind climates during the field works: **a** waves origin according to the significant height ( $H_s$ ) for the Bréhat station (~110 km Southwest of Alderney Race) and for the station 1 (location Fig. 1) and Wind origin from the Météo-France measurements in Goury semaphore; **b** times series of the conditions evolution during the field work: top, water level evolution (m.s.l.: mean sea level); middle, significant wave height ( $H_s$ , Bréhat station and ADCP-V data; station 1) and bottom, wind intensity in Goury

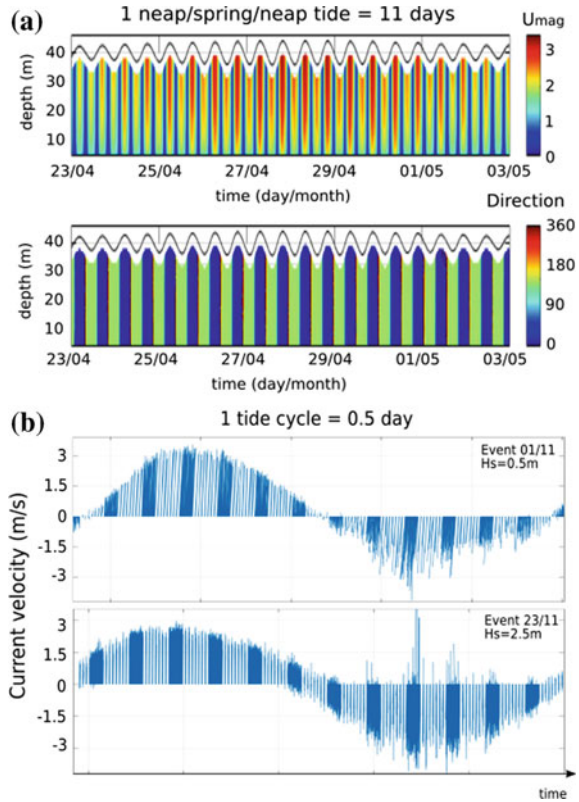
(Fig. 2b), the peak wind reached  $23 \text{ m.s}^{-1}$  and the maximum  $H_s$  was 4.3 m in Bréhat and 3.5 m in our study area (Fig. 2b).

### Current Evolution During a Typical Tidal Cycle

The evolution of current velocities in the Alderney Race area follows a progressive tidal wave regime. The maximum velocities are recorded during the high and low tide and not during the flood and ebb (Fig. 3a). One typical tidal cycle is showed in Fig. 3b.

A first current velocity peak is registered during the high tide with an averaged direction toward the NNE (~N20°) for the three stations. Subsequently, the velocity

**Fig. 3 a** Spatial-temporal diagrams of the  $U_{mag}$  (top) and direction (bottom) during the first neap/spring tide (April/May 2017); **b** Fishbone diagram of measured current vectors at station 2 during two events: 01 and 23 November 2017

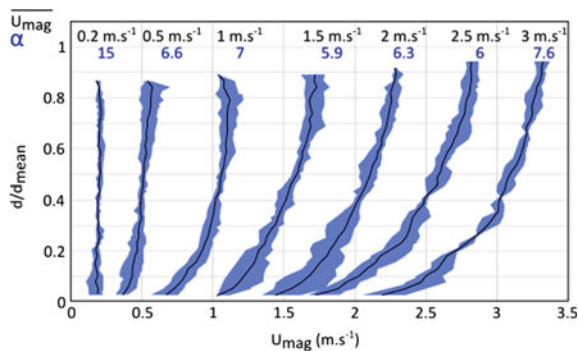


decreases during the first half of the ebb until it reaches a value close to  $0.1 \text{ m}\cdot\text{s}^{-1}$  (Fig. 3b). Current velocities increase again progressively in the opposite direction, toward the SSW ( $N190^\circ$ ) until the low tide, when a second velocity peak is recorded. Then the current velocities decrease until the half flood and a new tidal cycle start. The current inversions in the tide cycle is characterized by quasi-instantaneous clockwise current rotation. The maximal mean  $U_{mag}$  recorded are correlated with the tidal range (Fig. 3a). In the area, the highest measured of mean  $U_{mag}$  over the water column reaches  $3 \text{ m}\cdot\text{s}^{-1}$  during the high tide with the higher tidal range of  $7.8 \text{ m}$  (data averaged for  $5 \text{ min}$ ). In neap tide conditions (tidal range  $< 1.8 \text{ m}$ ), the velocities during the high tide are relatively lower, around  $1.8 \text{ m}\cdot\text{s}^{-1}$ . As shown in Fig. 1, the measurement site is located to the south of the maximal current zone of Alderney Race. However, during the acquisition period, and for all winds, waves and tides conditions,  $U_{mag}$  during high and low tide is always higher than  $1 \text{ m}\cdot\text{s}^{-1}$ .

**Vertical Profile Variations During Different Tide Phases**

Firstly, the  $\alpha$  coefficient have been calculated, using five minutes averaged data windows. However, when  $U_{mag}$  is lower than  $0.5 \text{ m}\cdot\text{s}^{-1}$  for all the water column, the associated profiles are relatively linear and this induces high values for the  $\alpha$

**Fig. 4** Graph shows seven vertical profiles corresponding to mean velocity (from 0.2 to 3  $\text{m}\cdot\text{s}^{-1}$ ). The blue values correspond to the estimated alpha



coefficient (for 0.2  $\text{m}\cdot\text{s}^{-1}$  the  $\alpha$  coefficient is up to 15, Fig. 4). Therefore, we removed all the profiles when  $U_{mag}$  is lower than 0.5  $\text{m}\cdot\text{s}^{-1}$  for the calculation of the average of the  $\alpha$  coefficient. This gives an average value equals to 6.6 ranging from 4 to 12, as in the study of Gooch et al. (2009).

Secondly, we have studied the relationships between the shape of the vertical profiles and the averaged velocity in the water column. We chose eight different cases for seven different averaged velocities (0.2; 0.5; 1; 1.5; 2; 2.5 and 3  $\text{m}\cdot\text{s}^{-1}$ , Fig. 4). The selection criteria in Fig. 4 where the  $U_{mag}$  averaged equal to the defined velocity at more and less 3% (blue envelop). Then, all the profiles have been merged and the  $\alpha$  coefficient have been calculated (Fig. 4). The graph in Fig. 4 shows that for a given averaged velocity, all the profiles display a relatively similar shape, but the variability of  $\alpha$  is too important to infer a correlation. In addition, there is no direct apparent relationship between the  $\alpha$  coefficient and the increase of  $U_{mag}$  (Fig. 4).

Thirdly, we calculated the average for the  $\alpha$  coefficient only in windows of 15 min during the different tide phases and specially around the velocity peak during high and low tide. This gives a value of 7.4 for the coefficient during high tides and value of 8.3 for the low tides. This difference between the  $\alpha$  values indicates a more bended profile and a more developed boundary layer for high tides compared with low tides. Such tendency is corroborated by the analyses of the velocity gradients between the sea bed and the surface, showing stronger gradient during high tide and more generally, when the velocity increases.

### Preliminary Observations on the Waves/Current Interaction

Two cases are presented here: the 01st and 23rd November 2017 cases showing a tidal range of 5.5 m and 5 m (see Table 2 and Fig. 2b). These events have been chosen because their tidal ranges are similar. They occurred close to each other in time and the difference between their  $H_s$  is significant. Other interesting events have been identified but the associated data are still in processing.

During the first case, the significant wave height reaches only 0.5 m, while  $H_s$  reaches 2.5 m during the second event (Table 2). For these two events, waves are coming from the northwest ( $N290^\circ$ ). For each case, we have selected two periods of 5 min showing two different current velocity situations, with averaged velocities



**Table 2** Characterization of events described and presented Fig. 5

Events (2017)	Tidal range (m)	$H_s$ (m)	Waves origin (°)	Current velocity $\overline{U_{mag}}$ ( $\text{m}\cdot\text{s}^{-1}$ )	Tide phase (current direction)
01/11	5.5	0.5	N290	0.36	Flood (NNE)
				2.25	Flood (NNE)
23/11	5	2.5	N290	0.36	Inversion (SSE)
				2.25	Flood (NNE)

$\overline{U_{mag}}$  of  $0.36 \text{ m}\cdot\text{s}^{-1}$  and  $2.25 \text{ m}\cdot\text{s}^{-1}$ . Three chosen events correspond to high tide phases with a main current direction toward the NNE (between  $\text{N}20^\circ$  and  $\text{N}42^\circ$  in average) and one event during the current inversion with a mean current direction toward the SE (case 23/11 with  $\overline{U_{mag}}$  of  $0.36 \text{ m}\cdot\text{s}^{-1}$ ). This selection of four events allows the comparison of different wave heights (0.5 m and 2.5 m) for the same current situation (for  $0.36 \text{ m}\cdot\text{s}^{-1}$  or for  $2.25 \text{ m}\cdot\text{s}^{-1}$ ) (Table 2). Figure 5 summarizes the  $U_{mag}$  and direction evolutions using spatial-temporal diagrams (during 5 min) for the four selected events. The velocity distribution using histograms at four selected depth (33 m, 23 m, 13 m and 3 m above the sea floor) is also represented for each event, the blue and red histograms correspond to low (0.5 m) and high (2.5 m)  $H_s$ , respectively.

For the low current velocity events ( $\overline{U_{mag}} = 0.36 \text{ m}\cdot\text{s}^{-1}$ ), the mean velocity profiles at  $0.2$  and  $0.5 \text{ m}\cdot\text{s}^{-1}$  (Fig. 4) shows that  $\overline{U_{mag}}$  only slightly varies in the water column. However, in details, the wave effect is clearly highlighted by  $U_{mag}$  variations in the almost whole water column (Fig. 5a) for the event with high  $H_s$  (2.5 m). In this case,  $U_{mag}$  vary from  $0.01$  to  $1.5 \text{ m}\cdot\text{s}^{-1}$  within a few seconds in the upper part of water column. The increase of  $U_{mag}$  ( $> 1 \text{ m}\cdot\text{s}^{-1}$ ) in this part is related to the wave propagation. The direction variations (Fig. 5a) are very significant for this case with an evolution from  $\text{N}50^\circ$  (NE), followed by a current directed to  $\text{N}180^\circ$  (S) up to  $\text{N}300^\circ$  (NW) between profiles separated by few seconds. These oscillations reach the bottom. The mean flow direction is toward the SSE but some local and brutal changes related with the waves occur. A period of 6–6.5 s can be calculated and the structures related with the waves are well defined. In these environmental conditions, waves have an important impact on the current. For the event with small  $H_s$  (0.5 m), the  $U_{mag}$  variation is lower with recorded variations of about  $0.5 \text{ m}\cdot\text{s}^{-1}$  in a few seconds. However, some oscillation structures are still visible in the first meters below the surface, meaning that the impact of waves in the water column for  $H_s$  of 0.5 m is not negligible when the mean tidal current is low ( $0.2 \text{ m}\cdot\text{s}^{-1}$ ) in the upper part of water column. These observations are confirmed by the distribution of current velocity on the histogram (Fig. 5a). The histogram distribution near surface 33 m above the bottom is wider than at 23, 13 and 3 m above the bottom (blue curve for  $H_s = 0.5 \text{ m}$ ). For the event with high  $H_s$  (red curve) the distribution near surface is very spread out compared with low  $H_s$  (from 0 to  $2 \text{ m}\cdot\text{s}^{-1}$ ). This spreading decreases with

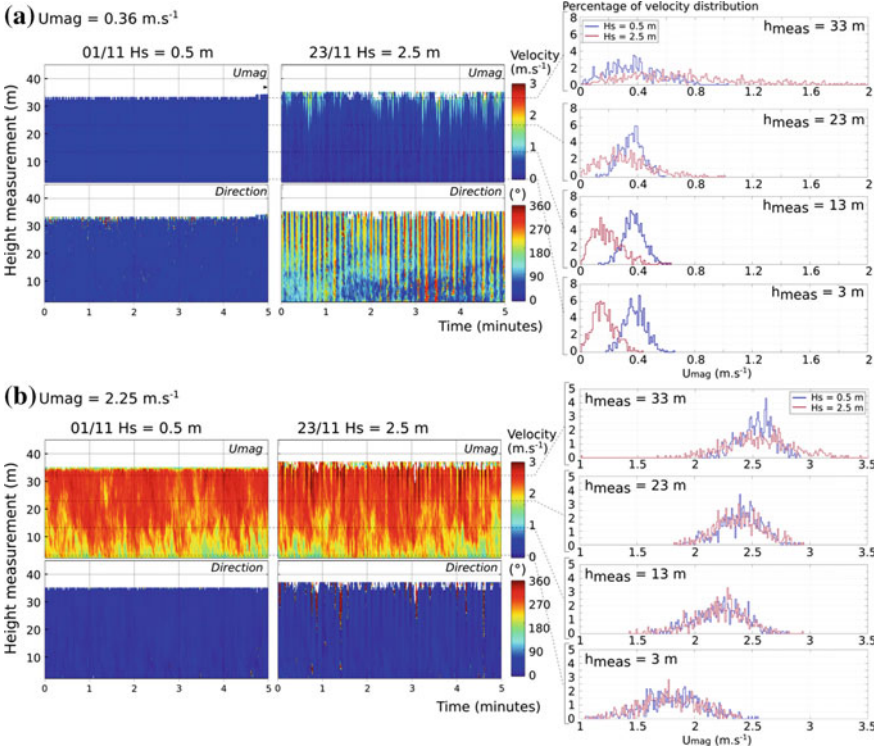


**Fig. 5** Data for the four studied cases: two events with different current velocity situations are selected during 5 min: **a**  $\overline{U}_{mag} = 0.36$  and **b**  $2.25 \text{ m.s}^{-1}$ . For each case, two moderate waves climate ( $H_s = 0.5 \text{ m}$  and  $H_s = 2.5 \text{ m}$ ) are presented. The spatio-temporal diagrams on the top of Fig. 5a, b are the  $U_{mag}$  and the direction on the sea bottom. On the right, histograms with velocity distribution at 33, 23, 13 and 3 m above the sea bed ( $h_{meas}$ )

depth and the distribution becomes more focused on the mean velocity. This mean velocity evolves in the water column from  $0.3 \text{ m.s}^{-1}$  at 23 m to  $0.15 \text{ m.s}^{-1}$  near the bottom, while it is expected to be centered on  $0.36 \text{ m.s}^{-1}$ . It may be explained by the fact that the mean velocity calculated at  $0.36 \text{ m.s}^{-1}$  take account the high velocity variation for waves propagation in the upper part of water column (Groeneweg and Klopman 1998).

For the high current velocities events (Fig. 5b  $\overline{U}_{mag} = 2.25 \text{ m.s}^{-1}$ ), the structures related with the waves propagation are relatively well defined when  $H_s$  is high (2.5 m case) in the upper part of water column and are absent when  $H_s$  is low (0.5 m case). For the low  $H_s$  (0.5 m), the current direction displays any dispersion compared with the events with low current velocities ( $0.36 \text{ m.s}^{-1}$  events), with only a direction variation of  $15^\circ$  (N15°–N30°, toward the NNE). When  $H_s$  is high,  $U_{mag}$  vary from 0 to  $1 \text{ m.s}^{-1}$  in few seconds in the upper part of water column. These variations are lower than the low current case. The period of the oscillations has been estimated at 6 s. The direction slightly varies between NNW (N350°) and NNE (N40°). In both

cases with low (0.5 m) and high (2.5 m)  $H_s$ , the low direction variation means that the current directions mainly reflect the tidal influence and not the wave effects, as the tidal currents during the high tide are focused toward the NNE. In addition, the histogram distributions are centered on mean velocity values that decrease with depth, following a power law, as shown in Fig. 4 in both cases. The histogram distribution of the upper measuring ADCP cell, near the surface is relatively wider (red curve) when  $H_s$  is high compared with the case of low  $H_s$ . This shows that waves with a height of 2.5 m are able to affected the upper water column, even when the tidal current are high ( $2.25 \text{ m.s}^{-1}$ ).

## 5 Conclusion and Perspectives

Three ADCP have been deployed in the Alderney Race area during thirteen neap/spring tide cycles. These data, which cover a long-time period allow the study of the current evolution at 1 or 2 Hz for several cycles. This chapter describes preliminary results concerning:

- (i) An estimation of the  $\alpha$  coefficient of 6.6 for all periods of measurement with a difference between the high and low tide phases. This value is close to the  $\alpha$  coefficient recommended in the literature (Frost et al. 2014).
- (ii) An important variability for the average velocity along vertical profiles (variations of  $U_{mag}$  from  $0.7$  to  $2.1 \text{ m.s}^{-1}$  in few seconds) that may be attributed to the tidal range, to the stage of tide, to the roughness of the sea floor, to the wind or the waves.
- (iii) A preliminary description of four events showing two different types of structures: an oscillation of the water particles linked with the waves in the upper part of the water column (but sometimes reaching the bottom) and turbulent structures probably linked with the roughness of the sea floor.

In a future work, we will quantify the influence of the waves on the tidal currents and the influence of the tidal currents on the orbital velocity of waves mainly in the cases of high currents and high waves. The important database collected allows us to study these processes for many events that will be presented in the future. In addition, the influence of the wind intensity and direction on the current characteristics will be also developed in future studies.

**Acknowledgements** Authors are supported by the HYD2M project (ANR-10-IEED-0006-07) funded by the program called “Investissements d’avenir” for the building of France Energies Marines. Authors acknowledge the crews of the ocean research vessels the CNRS vessels “Thalia” and “Côtes de la Manche”.

## References

- Bahaj, A. S., & Myers, L. E. (2004). Analytical estimates of the energy yield potential from the Alderney Race (Channel Islands), using marine current energy converters. *Renewable Energy*, 29, 1931–1945.
- Bailly du Bois, P., & Dumas, F. (2005). Fast hydrodynamic model for medium- and long-term dispersion in seawater in the English Channel and southern North Sea, qualitative and quantitative validation by radionuclide tracers. *Ocean Modelling*, 9, 169–210.
- Bailly du Bois, P., Dumas, F., Solier, L., & Voiseux, C. (2012). In-situ database toolbox for short-term dispersion model validation in macro-tidal seas, application for 2D-model. *Continental Shelf Research*, 36, 63–82.
- Coles, D. S., Blunden, L. S., & Bahaj, A. S. (2017). Assessment of the energy extraction potential at tidal sites around the Channel Islands. *Energy*, 124, 171–186.
- Foveau, A., Haquin, S., & Dauvin, J. (2017). Using underwater imagery as a complementary tool for benthos sampling in an area with high-energy hydrodynamic conditions. *Journal of Marine Biology Oceanography*, 6, 1–7.
- Frost, C., Evans, P. S., Morris, C. E., Mason-Jones, A., O’Doherty, T., & O’Doherty, D. (2014). The effect of axial flow misalignment on tidal turbine performance. In *Proceedings of 1st International Conference on Renewable Energies Offshore*.
- Gooch, S., Thomson, J., Polagye, B., & Meggitt, D. (2009). Site characterization for tidal power. In *OCEANS 2009, MTS/IEEE Biloxi-Marine Technology for Our Future: Global and Local Challenges*.
- Groeneweg, J., & Klopman, G. (1998). Changes of the mean velocity profiles in the combined wave—current motion described in a GLM formulation. *Journal of Fluid Mechanics*, 370, 271–296.
- Lewis, M., Neill, S., Robins, P., Hashemi, M., & Ward, S. (2017). Characteristics of the velocity profile at tidal-stream energy sites. *Renewable Energy*, 114, 258–272.
- Neill, S. P., Jordan, J. R., & Couch, S. J. (2011). *Impact of tidal stream turbines on sand bank dynamics* (pp. 2238–2245). Linköping, Sweden: World Renewable Energy Congress.
- Soulsby, R. L. (1977). Similarity scaling of turbulence spectra in marine and atmospheric boundary layers. *Journal of Physical Oceanography*, 7(6), 934–937.
- Thiébaut, M., & Sentchev, A. (2017). Asymmetry of tidal currents off W. Brittany coast and assessment of tidal energy resource around Ushant Island. *Renewable Energy*, 105, 735–747.
- Thiébot, J., Bailly du Bois, P., & Guillou, S. (2015). Numerical modeling of the effect of tidal stream turbines on the hydrodynamics and the sediment transport—Application to the Alderney Race (Raz Blanchard), France. *Renewable Energy*, 75, 356–365.
- Wiberg, P. L., & Sherwood, C. R. (2008). Calculating wave-generated bottom orbital velocities from surface wave parameters. *Computers & Geosciences*, 34(10), 1243–1262.